Available online at www.sciencedirect.com
ScienceDirect
Journal of Power Sources 180 (2008) 498–505
JOURNAL OF POWER SOURCES
www.elsevier.com/locate/jpowsour

Influence of different ruthenium(II) bipyridyl complex on the photocatalytic H_2 evolution over TiO_2 nanoparticles with mesostructures

Tianyou Peng [a,b,*], Dingning Ke [a], Ping Cai [a,**], Ke Dai [a], Liang Ma [a], Ling Zan [a]

[a] *College of Chemistry and Molecular Science, Wuhan University, Wuhan 430072, China*
[b] *Hubei Key Laboratory for Catalysis and Material Science, College of Chemistry and Material Science, South-Central University for Nationalities, Wuhan 430074, China*

Received 8 January 2008; received in revised form 1 February 2008; accepted 4 February 2008
Available online 12 February 2008

Abstract

H_2 production over dye-sensitized Pt/TiO_2 nanoparticles with mesostructures (*m*-TiO_2) under visible light ($\lambda > 420$ nm) was investigated by using methanol as electron donors. Experimental results indicate that three types of ruthenium(II) bipyridyl complex dyes (one binuclear Ru, two mononuclear Ru), which can be attached to Pt/*m*-TiO_2 with different linkage modes, show different photosensitization effects due to their different coordination circumstances and physicochemical properties. The dye tightly linked with *m*-TiO_2 has better durability but the lowest H_2 evolution efficiency, whereas the loosely attached dyes possess higher H_2 evolution efficiency and preferable durability. It seems that the dynamic equilibrium between the linkage of the ground state dye with TiO_2 and the divorce of the oxidization state dye from the surfaces plays a crucial role in the photochemical behavior during the photocatalyst sensitization process. It is helpful to improve the H_2 evolution efficiency by enhancing the electron injection and hindering the backward transfer. The binuclear Ru(II) dye shows a better photosensitization in comparison with mononuclear Ru(II) dyes due to its large molecular area, conjugation system, and "antenna effect", which, in turn, improve the visible light harvesting and electron transfer between the dye molecules and TiO_2.
© 2008 Elsevier B.V. All rights reserved.

Keywords: Hydrogen production; Photocatalyst; Sensitizer; Dye-sensitized titania

1. Introduction

A great number of attempts on photocatalytic splitting water into H_2 and/or O_2 by semiconductors (e.g. TiO_2 and CdS) have been made with a view to constructing solar energy conversion system to H_2 fuel from water, which is a clean chemical energy [1–5]. As a widely applied photocatalyst, TiO_2 absorbs only UV light with low quantum efficiency due to its wide energy gap (*ca.* 3.2 eV). The development of photocatalyst that can effectively harvest the visible light in the sunlight is indispensable for the photocatalytic H_2 production. An important way to improve the photocatalytic efficiency of TiO_2 is coupling with other semiconductor with narrow energy gap (e.g. CdS and WO_3), and doping some elements (metal and/or nonmetal) into TiO_2. However, a reliable and reproducible photocatalyst of this type has seldom been established up till now [6].

As a strategy for the effective absorption of visible light, photosensitization of TiO_2 photoelectrode with adsorbed dye has been studied extensively in the dye-sensitized nanocrystalline solar cells (DSSCs), in which dye molecules acted like chlorophyll to collect energy and then transported it to the semiconductor [7]. Based on a similar consideration, a promising system for H_2 production is the photosensitized reduction of water over the dye-sensitized semiconductor. This photocatalytic H_2 production from photocatalyst aqueous suspension is carried out in the presence of a photosensitizer (dye) and a sacrificial electron donor (e.g. ethylenediaminetetraacetic acid (EDTA), HI or triethanolamine (TEOA) [8–13]) or nonsacrificial electron donor (e.g. IO_3^-/I^- or I_3^-/I^- shuttle redox mediator [14–16]). However, the electron transfer mechanism of the dye molecules in above suspension for the H_2 pro-

* Corresponding author at: College of Chemistry and Molecular Science, Wuhan University, Wuhan 430072, China. Tel.: +86 27 8721 8474; fax: +86 27 6875 4067.
** Corresponding author. Tel.: +86 27 8721 8474; fax: +86 27 6875 4067.
E-mail addresses: typeng@whu.edu.cn (T. Peng), applecaiping@163.com (P. Cai).

0378-7753/$ – see front matter © 2008 Elsevier B.V. All rights reserved.
doi:10.1016/j.jpowsour.2008.02.002

duction is different from that in the DSSCs [9–16]. Up till now, xanthene dyes (e.g. eosine bluish, uranine, rhodamine B, erythrosine, rose Bengal, eosin Y) [12,13], coumarin [17] and merocyanine dye [17,18] have been used as sensitizer of TiO_2 for the photocatalytic H_2 evolution. Some Ru(II) bipyridyl dyes (e.g. *cis*-$Ru(dcbpy)_2(SCN)_2$ (N3 dye) [14], $Ru(bpy)_3Cl_2$ [11], and $Ru(dcbpy)_3Cl_2$ [15,16]), which were applied in the DSSCs, have also been used as sensitizer of semiconductor with wide energy gap for the H_2 production from a suspension system.

Most of those dye molecules have no ability to oxidize water to O_2 and consequently are decomposed under irradiation in the absence of a sacrificial electron donor, since O_2 evolution from water, which requires abstraction of four electrons, is much more difficult than the kinetically simpler process of the H_2 evolution [8–13,19]. The inability to produce O_2 over sensitizer molecules has prevented the construction of dye-sensitized photocatalysts for photosplitting water into H_2 and O_2. Moreover, the firmly bound dye like N3 can be stabilized near the TiO_2 surfaces through its carboxyl groups, but the injected electrons in the conduction bands of TiO_2 also possibly transfer backward to the oxidized dye molecules [14–16], which results in the decrease of H_2 evolution. Whereas it was probable that the thermal reorientational motion of the loosely attached dye molecules enhanced the electron transfer as reported by Kajiwara et al. [11]. Therefore, it is still necessary to seek new, effective sensitizer for the H_2 production over semiconductor. To the best of our knowledge, there are still seldom investigations focused on the photosensitization of Ru(II) bipyridyl dyes attached to semiconductor with different linkage modes on the H_2 production [11,15,16], especially for the polynuclear Ru complex with "antenna effect", although trinuclear complexes such as $[Ru(bpy)_2(CN)_2]_2Ru(dcbpy)_2$ have been used as antenna-sensitizer in the DSSCs [7].

Titania (*m*-TiO_2) nanoparticles with mesostructures have been fabricated and shown much better photoactivity than that of the commercial photocatalyst P25 (TiO_2, Degussa, Germany) due to its high specific surface area and well-crystallized mesoporous wall as shown in our previous publications [20,21]. Recent results indicated that the as-synthesized *m*-TiO_2 with smaller crystallite size (2.3 nm) dispersed among the amorphous mesoporous domains showed the best photoactivity for the H_2 production among the various calcined *m*-TiO_2, which possess much higher crystallinity than the as-synthesized one [22]. Herein, the effect of hydrothermal temperature for the preparation of *m*-TiO_2 on the photocatalytic H_2 evolution under UV irradiation was investigated in detail, in order to further make it clear whether the amorphous domain is more beneficial for the H_2 evolution. And the photosensitization of three types of Ru(II) bipyridyl dyes ($Ru_2(bpy)_4L_1$-PF_6, $Ru(bpy)_2(him)_2$-NO_3 and (n-$Bu_4N)_2$-*cis*-$Ru(dcbpy)_2(SCN)_2$), which can be attached to *m*-TiO_2 through different linkage modes, were comparatively investigated. The effect of calcination temperature on the photocatalytic H_2 evolution efficiency over the Pt/*m*-TiO_2 sensitized with different dyes was also studied.

2. Experimental

2.1. Materials

$H_2PtCl_6{\cdot}6H_2O$ was obtained from a commercial source and used without further purification. The *m*-TiO_2 nanoparticles were prepared under different hydrothermal temperatures according to our previous publications [20,21]. The properties of the as-synthesized *m*-TiO_2 nanoparticles derived from hydrothermal treatment at 100 °C and its calcined products are listed in Table 1.

N719 [(n-$Bu_4N)_2$-*cis*-$Ru(dcbpy)_2(SCN)_2$], one of the best sensitizer for the DSSCs with the same structure as N3 dye [*cis*-$Ru(dcbpy)_2(SCN)_2$] [14], was purchased from Solaronix Co. and used as reference substance because it can be tightly bound to *m*-TiO_2 through its carboxyl group [7,14–16]. $Ru(bpy)_2(him)_2$-NO_3 and $Ru_2(bpy)_4L_1$-PF_6 were prepared by ourselves according to the previous literatures [23,24]. The two complexes do not have terminal group which can form tight linkage with semiconductor as N719 [11]. Among these, dcbpy = 2,2′-bipyridyl-4,4′-dicarboxylic acid, bpy = 2,2′-bipyridine, L = μ-4,4′-azo-benzene carboxylic acid, him = imidazole. The prepared samples were studied by using UV–vis spectrophotometer (Shimadzu, UV-2556). Fig. 1 gives the molecular structures of above three Ru(II) bipyridyl dyes.

2.2. Preparation process

Pt/*m*-TiO_2 photocatalysts were prepared through a photodeposition procedure as follows. 0.01 g $H_2PtCl_6{\cdot}6H_2O$ and 0.38 g *m*-TiO_2 nanopowders were added into 175 ml of 2.0 M Na_2CO_3 aqueous solution in the photoreaction cell (Pyrex glass) in sequence. And then this mixture was irradiated by a 500 W high-pressure Hg lamp for 5 h under stirring. During UV irradiation, H_2PtCl_6 was photoreduced to form highly dispersed Pt particles on the *m*-TiO_2 nanoparticles. The sample was separated by centrifugation and washed with water, and then dried at 120 °C overnight to obtain 1.0 wt.% Pt/*m*-TiO_2 nanoparticles. The obtained Pt/*m*-TiO_2 nanoparticles were immersed in 1×10^{-4} M dye aqueous solution for 72 h in dark room, then filtrated and washed with water several times, dried at 80 °C for 12 h to obtain the dye-sensitized Pt/*m*-TiO_2.

Table 1
Summary of the physicochemical properties of the *m*-TiO_2 nanoparticles [21]

Calcination temperatures (°C)	Crystal size (nm)	S_{BET} ($m^2\ g^{-1}$)	Mean pore size (nm)	Total volume ($cm^3\ g^{-1}$)
As-synthesized	2.3	438.3	2.1	0.56
300	2.9	330.5	2.3	0.59
500	4.1	232.7	2.5	0.53

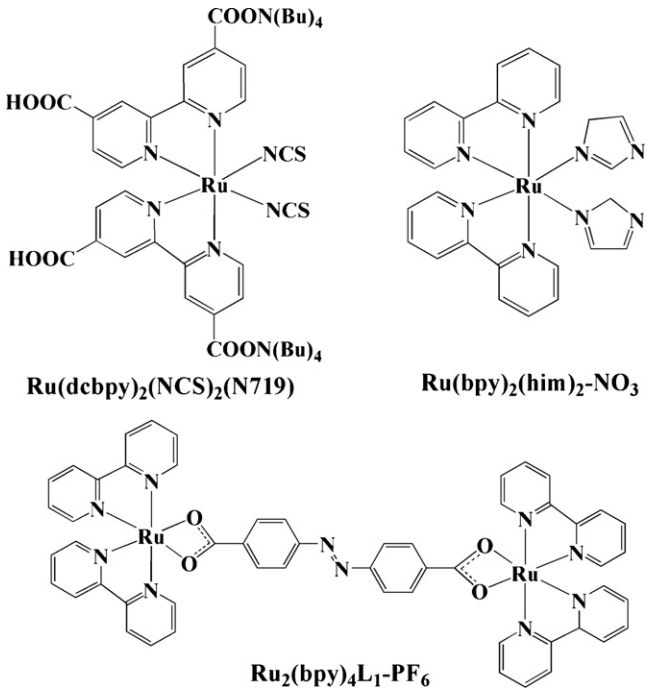

Fig. 1. Molecular structures of the three ruthenium(II) bipyridyl complex dyes.

2.3. Photocatalytic process

The H_2 production reactions were carried out in an outer irradiation-type photoreactor (Pyrex glass) connected to a closed gas-circulation system. A 250 W Xe lamp (Beijing Trusttech Co. Ltd., Beijing, China) was afforded as light source, which was collimated and focalized into 5 cm^2 parallel faculae, then translated into uprightness light by a viewfinder. A cutoff filter (Kenko, L-42; $\lambda > 420$ nm) was employed to obtain visible light irradiation. The reaction was performed in distilled water (80 ml) and methanol (20 ml) solution containing the dye-sensitized Pt/*m*-TiO_2 (40 mg), then the suspension was thoroughly degassed to remove air, and the reactor was irradiated from the top with the visible light ($\lambda > 420$ nm). Rate of H_2 evolution was analyzed with an online gas chromatograph (GC, SP-6800A, TCD detector, 5 Å molecular sieve columns and Ar carrier).

3. Results and discussion

3.1. Optimization of the hydrothermal temperature

Our previous results indicated that the as-synthesized Pt/*m*-TiO_2 nanoparticles, which has large specific surface area (438 $m^2\ g^{-1}$) and semicrystallite (2.3 nm) within the amorphous mesoporous domains (particle size, *ca.* 20 nm) [20,21], showed the best photocatalytic activity for the H_2 production under UV irradiation among the products calcined at elevated temperatures, and this photoactivity decreased with enhancing the calcination temperature [22]. In other words, the as-synthesized *m*-TiO_2 with a lower crystallinity possesses a better H_2 evolution efficiency than the calcined products with a higher crystallinity. It is clearly different from the previous reports [25–27]. To further confirm whether the amorphous mesoporous domain is more beneficial for the photocatalytic H_2 evolution, three types of *m*-TiO_2 nanoparticles were synthesized from different hydrothermal temperatures according to our previous publication [20]. Fig. 2 depicts the XRD patterns of the as-synthesized samples derived from hydrothermal treatment at 60, 100 and 200 °C, respectively. As can be seen, the diffraction peaks of anatase become stronger and sharper upon enhancing the hydrothermal temperature, indicating the improved crystallinity of the as-synthesized *m*-TiO_2 after an ion-exchange process and drying at 80 °C.

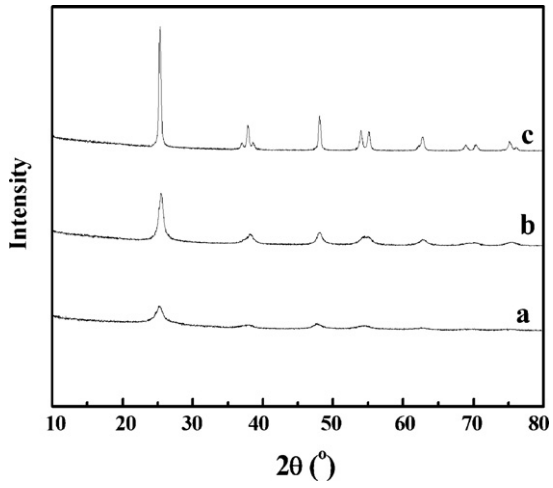

Fig. 2. XRD patterns of the *m*-TiO_2 derived from different hydrothermal temperatures: (a) 60 °C, (b) 100 °C, and (c) 200 °C.

Table 2 shows the photocatalytic H_2 evolution rates over the as-synthesized Pt/*m*-TiO_2 derived from different hydrothermal temperature under UV irradiation (Hg lamp as light source) as described previously [22]. From Table 2, the H_2 evolution rate increases from 3511 to 9112 $\mu mol\ g^{-1}\ h^{-1}$ when the hydrothermal temperature is enhanced from 60 to 100 °C and then decreases to 5346 $\mu mol\ g^{-1}\ h^{-1}$ upon further enhancing it to 200 °C. The *m*-TiO_2 derived from 100 °C shows the highest H_2 evolution rate among the three products, whereas the sample derived from 200 °C with a higher crystallinity shows a lower H_2 evolution rate than that derived from 100 °C. These results indicate that more amorphous domains are not beneficial for the improvement of the photocatalytic H_2 evolution. Namely, the high surface area and the semicrystallite within the mesoporous walls play important roles in the H_2 evolution as described before [22]. The exact reason for this observation is still unclear, which should be further investigated.

Table 2
Photocatalytic H_2 production over the as-synthesized Pt/*m*-TiO_2 derived from different hydrothermal temperatures under UV irradiation

Hydrothermal temperature (°C)	Rate of H_2 production ($\mu mol\ g^{-1}\ h^{-1}$)
60	3511
100	9112
200	5346

Conditions: catalyst amount 40 mg 1.0 wt.% Pt/*m*-TiO_2, methanol amount 30 ml, light source 500 W Hg lamp, and irradiation time 150 min.

On the basis of the previous investigations, however, we can give some general assumptions to explain the above experimental results. It is well known that the particle size, specific surface area, porosity, crystallinity and crystal phase of TiO_2 play important roles in its photoactivity. Most of the reports indicated that the transfer time of the photogenerated carriers to the surface of TiO_2 was proportionate to the dimension of the crystallite size [20,28]. Therefore, the smaller the crystallite size of photocatalyst is, the more photogenerated electrons move to the surfaces of TiO_2 and, in consequence, the more electrons participate in the redox reaction of water or organic substance. In addition to the crystallite size, the specific surface area of TiO_2 and the dispersity of the co-catalyst (e.g. Pt) also influence significantly the H_2 evolution efficiency [25,27–29]. In the present experimental conditions, the crystallinity of *m*-TiO_2 was improved concomitantly with the decrease in the amorphous domains upon enhancing the hydrothermal temperature, which can provide more active sites for the H_2 production. This can explain why the samples derived from 100 and 200 °C show higher H_2 evolution rates than those derived from 60 °C. Once the hydrothermal temperature is higher than 100 °C, the crystallite sizes are much larger than those in the samples derived from 100 °C as shown in Fig. 2. It is not beneficial for the fabrication of stable mesostructures of *m*-TiO_2 with large specific surface area, which can lead to the increase in the transfer time of the photogenerated carriers in *m*-TiO_2 and the recombination probability, and then to the decrease of the H_2 production rate. Therefore, the *m*-TiO_2 nanoparticles used in the following section were prepared from hydrothermal treatment at 100 °C [20].

3.2. UV–vis absorption spectra of dyes

The firmly bound dyes can be stabilized near the TiO_2 surfaces, and lead to a fast electron injection of the excited state dyes into substrate because the probability of this process depends on the overlap of the wave functions of the donor and the acceptor [11,30], but the injected electrons in the conduction bands of TiO_2 also possibly backward transfer to the oxidized dye molecules due to its tight linkage with TiO_2 [30]. Moreover, it is probable that the thermal reorientational motion of the loosely attached dye molecules can enhance the electron transfer [11]. On the basis of the aforementioned discussions on the effect of linkage mode between the dye and substrate on the electron transfer, we thus conjectured that the dynamic equilibrium between the linkage of dye with TiO_2 and the divorce of the oxidization dye from the surfaces could be beneficial for injecting excited electrons into TiO_2 and hindering the backward transfer, and then improve the light quantum efficiency. Therefore, we selected three types of dyes as described above, which possess different ligand terminal groups and can be linked with TiO_2 through different modes, to compare their photosensitization. Thereinto, N719 can be firmly linked with TiO_2 through its carboxyl group [15], while the other dyes do not have terminal group like carboxyl and can only be loosely attached to TiO_2. The binuclear Ru dye is also selected to investigate the validity of the "antenna effect" of dye on the photocatalytic H_2 evolution [7].

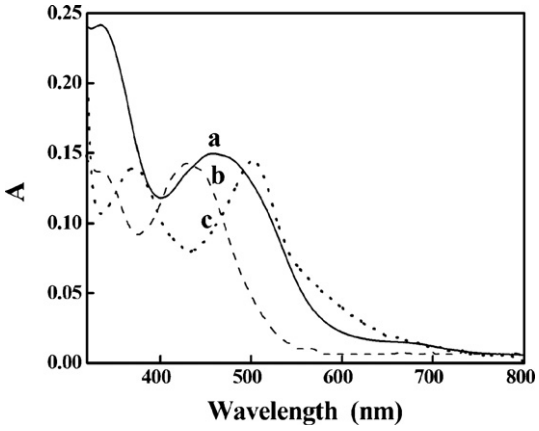

Fig. 3. UV–vis absorption spectra of the three ruthenium(II) bipyridyl complex dyes: (a) $Ru_2(bpy)_4L_1$-PF_6; (b) $Ru(bpy)_2(him)_2$-NO_3; (c) N719.

Fig. 3 shows the UV–vis spectra of three Ru(II) bipyridyl complexes aqueous solutions. The corresponding maximum absorption wavelengths in the visible light region for $Ru_2(bpy)_4L_1$-PF_6, $Ru(bpy)_2(him)_2$-NO_3 and N719 are 456, 436 and 502 nm, respectively. The binuclear $Ru_2(bpy)_4L_1$-PF_6 shows the broadest absorption band in the visible region due to its large molecular area and delocalized conjugation system, although its maximum absorption wavelength is slightly shorter than that of N719 because of the presence of carboxyl groups. Moreover, mononuclear $Ru(bpy)_2(him)_2$-NO_3 also possesses a large molecular area and conjugation system as indicated in Fig. 1, it also shows a broader absorption band in the visible light region although its maximum absorption wavelength is much shorter than N719. These optical physical properties of $Ru(bpy)_2(him)_2$-NO_3 and $Ru_2(bpy)_4L_1$-PF_6 are beneficial for the visible light absorption and the electron injection of excited state dye under the visible light irradiation [7,11].

Ru(II) bipyridyl complexes such as N719 and N3 dyes have been studied as sensitizers to harvest the visible light in the DSSCs consisting of dye-sensitized TiO_2 photoelectrode and an I_3^-/I^- redox couple in an organic solvent [31,32]. The results indicated that these dyes have suitable ground states (HOMO) and excited states (LUMO) for the efficient electron transfer. That is, electron injection from an excited state dye to the conduction bands of TiO_2 occurs efficiently due to the firm linkage through their terminal carboxyl groups. For the photocatalytic H_2 production over the present Pt/*m*-TiO_2 suspension, however, the solution must contain some sacrificial electron donors due to the lack of I_3^-/I^- shuttle redox mediator, otherwise Ru(II) dyes might be decomposed during the visible light irradiation. Therefore, the H_2 evolution rate was tested in water–methanol suspension containing the dye-sensitized Pt/*m*-TiO_2 in the following sections.

3.3. Effect of dye sensitization on H_2 evolution over the Pt/m-TiO_2

Primary experimental results showed that there was no obvious H_2 production over the as-synthesized Pt/*m*-TiO_2 with/without dye sensitization under the visible light irradi-

Table 3
Photocatalytic H_2 evolution efficiency over the dye-sensitized Pt/*m*-TiO_2 nanoparticles

Dye-sensitized *m*-TiO_2	300 °C calcined ($\mu mol\ g^{-1}\ h^{-1}$)	500 °C calcined ($\mu mol\ g^{-1}\ h^{-1}$)
$Ru_2(bpy)_4L_1$-PF_6	1018.7	974.1
$Ru(bpy)_2(him)_2$-NO_3	694.3	675.1
N719	308.9	242.3
Without sensitization	0	0

Conditions: distilled water 80 ml, methanol 20 ml, dye-sensitized 1.0 wt.% Pt/*m*-TiO_2 40 mg, irradiated from the top with $\lambda > 420$ nm visible light, and irradiation time 1 h.

ation ($\lambda > 420$ nm). It indicated that the band gap excitation did not occur due to the low energy of visible light. For the as-synthesized *m*-TiO_2, its semicrystallite was located in the amorphous domains, and the excited state electrons of dye cannot efficiently inject into the semicrystallites due to the obstruction of the surrounding amorphous domain and the large dye molecular structure, which result in no obvious photosensitization on the Pt/*m*-TiO_2. Therefore, we focused on the effects of the three dyes on the H_2 evolution over the Pt/*m*-TiO_2 after calcinations at 300 and 500 °C. The porous walls of *m*-TiO_2 nanoparticles can be completely crystallized into anatase with limited damage and/or collapse of the mesostructures after calcinations at 300 and 500 °C as shown in Table 1 and our previous investigations [20,21].

Table 3 shows the photocatalytic H_2 evolution rates over the calcined Pt/*m*-TiO_2 loaded with different dyes under the visible light irradiation for 1 h. All dyes used here show obvious photosensitization on the H_2 evolution, indicating that the dyes can be efficiently excited and the excited state electrons can be injected into the conduction bands of *m*-TiO_2, and then transported to the loaded Pt to produce H_2. The H_2 evolution rate over the dye-sensitized Pt/*m*-TiO_2 after calcinations increases according to N719 < $Ru(bpy)_2(him)_2$-NO_3 < $Ru_2(bpy)_4L_1$-PF_6. For the Pt/*m*-TiO_2 calcined at 300 °C, the H_2 evolution rates over $Ru_2(bpy)_4L_1$-PF_6 and $Ru(bpy)_2(him)_2$-NO_3 sensitized products are about 3.30 and 2.18 times as that of N719 sensitized sample, respectively. Abe et al. have demonstrated that the H_2 evolution rate decreased with reducing the energy gap between the redox potential of I_3^-/I^- and the HOMO levels of dye, which can depress the electron transfer efficiency from I^- to dye [14]. However, this difference in the energy gap (between redox potential of methanol and HOMO levels of dye) should be small due to their similar metal centers and ligands in the three dyes, indicating that the suggestion stated above cannot apply entirely to the present case.

As shown in Figs. 1 and 3, the present three dyes have similar Ru(II) centers but with different coordination environments and physicochemical properties. For example, N719 molecules have carboxyl groups, which can be tightly linked with *m*-TiO_2 [14–16], while $Ru_2(bpy)_4L_1$-PF_6 does not have terminal group like carboxyl and can only be loosely attached to TiO_2 through oxygen bridge bonds derived from the reaction of surface hydroxyl of TiO_2 and the four oxygen atoms with the delocalized π bond from the azo-benzene carboxylic spacer (L). Similarly, $Ru(bpy)_2(him)_2$-NO_3 can only be loosely attached to TiO_2 through hydrogen bonds from the un-coordinated N atom in imidazoles and the surface hydroxyl of TiO_2. Moreover, $Ru_2(bpy)_4L_1$-PF_6 and $Ru(bpy)_2(him)_2$-NO_3 possess large conjugated systems and molecular areas, which result in much broader absorption bands in the visible region than N719. We thus presumed that the differences in the photosensitization among the three dyes could be attributed to their different coordination circumstances and physicochemical properties which can influence the interaction between TiO_2 and dye, the visible light absorption and electron transfer, and then the H_2 evolution [10–13].

On one hand, the highest H_2 evolution efficiency over the $Ru_2(bpy)_4L_1$-PF_6 sensitized Pt/*m*-TiO_2 can be ascribed to the more effective visible light harvesting and electron transfer [8–13]. First, the excited state electrons of this dye can be transferred through two ways, MLCT (metal-to-ligand) and MMCT (metal-to-metal), while the mononuclear Ru(II) dyes ($Ru(bpy)_2(him)_2$-NO_3 and N719) conduct a single electron transfer way (MLCT). Namely, the electron transportations also take place between the two Ru centers connected by the delocalized conjugated system. Amadelli et al. have reported that two $Ru(bpy)_2(CN)_2$-units in a trinuclear dye [$(Ru(bpy)_2(CN)_2)_2Ru(dcbpy)_2$] absorbed light energy and transported to the other $Ru(dcbpy)_2$-unit connected with TiO_2 through tight chemical bonds [7]. This outside $Ru(bpy)_2(CN)_2$-units played a role of antenna and IPCE was more than 80%. According to this view, "antenna effect" must exist in the $Ru_2(bpy)_4L_1$-PF_6 sensitized Pt/*m*-TiO_2 system, which is beneficial for the visible light absorption. Secondly, one $Ru(bpy)_2$-unit in this dye can first absorb the visible light and transport it to the other $Ru(bpy)_2$-unit (MMCT) through the azo-benzene carboxylic spacer, and then the excited state electrons can be effectively transferred to the conduction bands of *m*-TiO_2 through the oxygen bridge bonds between this dye molecules and *m*-TiO_2. Finally, the other $Ru(bpy)_2$-unit directly linked with *m*-TiO_2 can also harvest the visible light and transfer the excited electrons to *m*-TiO_2 (MLCT). This synergetic effect of above two ways accelerates the visible light harvesting and the electron transfer between $Ru_2(bpy)_4L_1$-PF_6 and *m*-TiO_2.

On the other hand, N719 should theoretically show much better photosensitization than the other two dyes due to its smaller molecular area and the much strong chemical fixation, which is beneficial for the adsorption of dye and the electron injection. However, N719 shows the lowest photosensitizing effect on the Pt/*m*-TiO_2 among the three dyes tested. These can be attributed to the following factors. First, the calcined *m*-TiO_2 still possesses comparatively high surface area and porosity as shown in Table 1, the adsorption amount of dye is not the key factor on the visible light harvesting. Whereas the large conjugated systems and molecular areas of $Ru_2(bpy)_4L_1$-PF_6 and $Ru(bpy)_2(him)_2$-NO_3 feature in the visible light harvesting and electron injection. As for the binuclear Ru(II) dye, its "antenna effect" dominates in comparison with the adsorption amount of dye molecules. Secondly, N719 was tightly linked to TiO_2 through the carboxyl group and its six atoms of the pyridine ring on one plane, therefore the injected electrons can also be backward transferred to

the oxidized dye molecules [30]. Namely, N719 has a higher possibility of the recombination reaction during the photochemical reaction. Whereas this electron backward transfer and recombination can be hindered due to the loose linkage between the other two dyes and *m*-TiO_2, because the coordination circumstances of Ru centers need to change in order to meet with the change in the valence state after the electrons injected into TiO_2. This likely means the change in the linkage mode and the divorce of the oxidized dyes from TiO_2. Anyway, those loose interactions such as oxygen bridges and hydrogen bonds might act as the carboxyl linkage between N719 and TiO_2 to promote the electron injection, and the oxidized dye molecules can divorce timely from TiO_2 to avoid the backward transfer, which results in more effective light harvesting and higher quantum efficiency.

It seems reasonable to conclude that the H_2 evolution efficiency is related not only to the linkage modes between the dyes and TiO_2, but also to the coordination circumstances and physicochemical properties of Ru(II) dyes, which affect the visible light harvesting and the electron transfer efficiency. The dynamic equilibrium between the linkage of the ground state dye with TiO_2 and the divorce of the oxidized dye from the surfaces seems to be beneficial for injecting the excited state electrons into TiO_2 and hindering the injected electrons backward transfer to the oxidized dye, which can improve the light quantum efficiency and H_2 evolution efficiency.

3.4. Effect of calcination temperature on the H_2 evolution over dye-sensitized Pt/m-TiO_2

To study the reproducibility of the H_2 production over the dye-sensitized Pt/*m*-TiO_2 after calcination at different temperatures, we have measured the H_2 evolution rate every 1 h of visible light irradiation, in which the next portion of methanol (10 ml) was added into the same suspension. Fig. 4 shows the time course of H_2 evolution over the dye-sensitized Pt/*m*-TiO_2 after calcinations at 300 and 500 °C. As can be seen, the H_2 evolution rate decreases upon enhancing the calcination temperature from 300 to 500 °C. The *m*-TiO_2 calcined at 300 °C possesses comparatively higher specific surface area, smaller nanocrystallite located in the well-defined mesoporous domains than the product calcined at 500 °C [20,21]. These characteristics in microstructures of *m*-TiO_2 calcined at 300 °C mean more effective and faster charge transfer as well as uniform dispersion of the co-catalysts (Pt) and dye molecules, which, in turn, lead to a higher H_2 evolution efficiency in comparison with the product calcined at 500 °C. As for the *m*-TiO_2 calcined at 500 °C, $Ru_2(bpy)_4L_1$-PF_6 still shows a better photosensitization than $Ru(bpy)_2(him)_2$-NO_3 and N719.

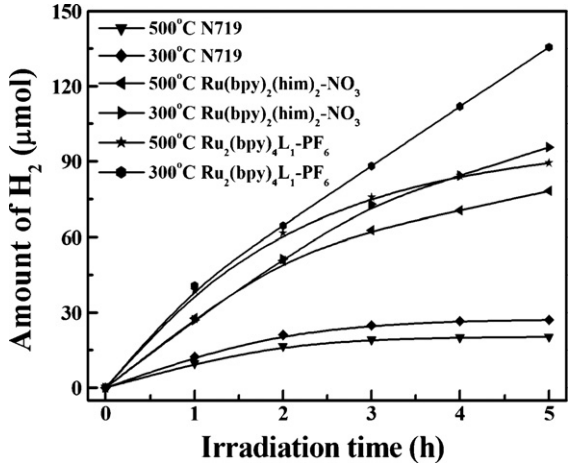

Fig. 4. Time courses of the photocatalytic H_2 production over the dye-sensitized Pt/*m*-TiO_2 nanoparticles.

With enhancing the calcination temperature from 300 to 500 °C, the decreasing trend in H_2 evolution over the *m*-TiO_2 increases according to N719 < $Ru(bpy)_2(him)_2$-NO_3 < $Ru_2(bpy)_4L_1$-PF_6 after 3 h irradiation. The higher durability of N719 can be ascribed to its tight linkage with TiO_2 though it still shows a far lower H_2 evolution rate. Previous results demonstrated that the tightly fixed dye is beneficial for the improvement in the stability and reproducibility of the dye-sensitized TiO_2 [11,13–16]. For example, Abe et al. have reported eosin Y-fixed TiO_2 using a silane-coupling reagent [13], and found that the H_2 evolution reproduced even after the exchange of TEOA aq., while the H_2 evolution from the mixture of eosin Y and Pt/TiO_2 ceased in 10 h. Osa and Fujihira have also reported a photoelectronchemical cell consisted of rhodamine B and TiO_2 electrode, in which the dye was chemically fixed via amide bonding on semiconductor surfaces using silane-coupling reagent [33]. Those fixation methods via chemical bonding are more suitable for dye-sensitized photocatalyst used in aqueous solutions, because it is more resistant to oxidization of the dyes in water. However, all $Ru_2(bpy)_4L_1$-PF_6 and $Ru(bpy)_2(him)_2$-NO_3 sensitized samples exhibit more steady and higher increase in the H_2 evolution upon prolonging the irradiation time from 0 to 5 h, while the H_2 evolution rate for the N719 sensitized Pt/*m*-TiO_2 almost remain unchangeable after 3 h irradiation as shown in Fig. 4. Moreover, at all tested irradiation periods, the H_2 evolution rates over $Ru_2(bpy)_4L_1$-PF_6 and $Ru(bpy)_2(him)_2$-NO_3 sensitized Pt/*m*-TiO_2 are much higher than that over N719 sensitized one. Namely, the tightly bound N719 possesses several advantages such as durability and less influence of pH, but it shows the worst photosensitization in comparison with the loosely linked $Ru_2(bpy)_4L_1$-PF_6 and $Ru(bpy)_2(him)_2$-NO_3 in the present case. This more steady and higher increase in H_2 evolution for $Ru_2(bpy)_4L_1$-PF_6 and $Ru(bpy)_2(him)_2$-NO_3 sensitized Pt/*m*-TiO_2 can be ascribed to their stable chemical structures, the lower risk of the backward electron transfer and/or even the photodegradation due to their oxidized dye molecules can be timely disengaged from the nanoparticles as described above.

The differences in photosensitization can also be ascribed to the H_2 production mechanism among the three dyes sensitized products. In the case of $Ru_2(bpy)_4L_1$-PF_6 and $Ru(bpy)_2(him)_2$-NO_3, the dye molecules just are loosely linked with TiO_2, which provides an opportunity of H_2 production caused by the direct electron transfer from the excited state dye to Pt metal in addition to the electron transfer through oxygen bridges or hydrogen bonds to TiO_2 and then to Pt metal [13]. For example, H_2 evolutions proceed in the presence of dye, TEOA and colloidal Pt,

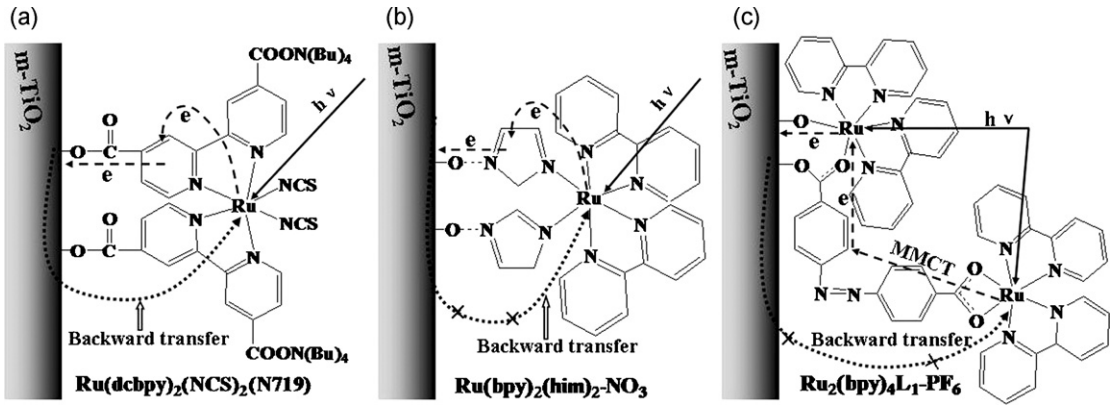

Fig. 5. Photoinduced electron transfer cycle in the three types of dyes sensitized Pt/*m*-TiO_2 nanoparticles.

because of the high reducing power and long-lived nature of the semi-reduced dye [13]. However, in the N719 sensitized product through the tight linkage, the electron transfer mainly takes place through the conduction bands of TiO_2 and then to Pt [14–16]. Therefore, we can think that the durability and reproducibility of H_2 production over the dye-sensitized Pt/*m*-TiO_2 are related not only to the linkage mode between the dye and semiconductor surface, but also to the photochemical behavior in the present case, which will be further discussed in the next section.

3.5. Discussion on the photochemical behavior in the dye-sensitized Pt/m-TiO_2 suspension

The photocatalytic H_2 evolution observed from the dye-sensitized Pt/*m*-TiO_2 suspension indicated that the photoelectron injection did occur in the present system. The mononuclear and binuclear Ru dyes are expected to adsorb on the surfaces of *m*-TiO_2 in comparable amounts due to their similar coordination centers and ligands. Therefore, the discussions on the photoinduced electron transfer cycle in the dye-sensitized *m*-TiO_2 suspension system are beneficial for understanding the different photosensitization among the three dyes. As described above, the tightly linked N719 would be stabilized near the surface of *m*-TiO_2. This stabilization would be larger in the ground state than that in the excited state because the adsorbed molecules in the ground state locate the position of minimum energy on the surface [11]. However, our experimental results show that N719 gives the lowest photosensitization on the present *m*-TiO_2 in comparison with $Ru_2(bpy)_4L_1$-PF_6 and $Ru(bpy)_2(him)_2$-NO_3. Therefore, it is reasonable to conclude that there exists different electron transfer mechanism between the tightly bound dye and loosely attached dyes. A schematic representation of the electron transfer processes that take place in the dye-sensitized *m*-TiO_2 suspension is shown in Fig. 5.

As mentioned above, for the firmly bound N719 sensitized *m*-TiO_2, the injected electron in TiO_2 can be also backward transferred to the oxidized dye as shown in Fig. 5a [7,11,30], which result in reducing the quantum efficiency. While $Ru_2(bpy)_4L_1$-PF_6 and $Ru(bpy)_2(him)_2$-NO_3 are loosely attached to TiO_2 through the oxygen bridge and hydrogen bond as shown in Fig. 5b and c, respectively. Those loose linkages are beneficial for the electron injection of the excited state dyes into TiO_2, in the meanwhile, the electron backward transfer can be effectively hindered due to the divorce of the oxidized dyes from the TiO_2 surfaces as described in Section 3.3. Namely, an electron of dye is injected into the TiO_2 by excited state MLCT, and immediately the oxidized dye is disengaged from the TiO_2, then the ground state dye is regenerated by electron transfer from methanol and links with *m*-TiO_2 again to conduct a new cycle. On the basis of aforementioned discussions, the photochemical behavior and electron transfer cycle in $Ru_2(bpy)_4L_1$-PF_6 or $Ru(bpy)_2(him)_2$-NO_3 sensitized TiO_2 can be induced as follows: dyes fixation through loose linkage (oxygen bridge or hydrogen bond) → dye excitation ($h\nu$) → electron transfer (MLCT and/or MMCT) → electron injection (directly to Pt and/or through TiO_2) → divorce of oxidized dye from *m*-TiO_2 (valence state change and coordination effect) → regeneration (obtain electron from methanol) → re-fixation to *m*-TiO_2.

The dynamic equilibrium between the linkage of the ground state dye molecules with TiO_2 and the divorce of the oxidized dye molecules from the surfaces seems to hinder the injected electrons backward transfer to the oxidized dye and improves the electron injection and light quantum efficiency. Whereas the tightly linked N719 is difficult to leave from TiO_2, which lead to the electron backward transfer as shown in Fig. 5a. Furthermore, the H_2 evolution rate over the N719 sensitized Pt/*m*-TiO_2 remaining unchangeable after 3 h irradiation as illustrated in Fig. 4 also implies the equilibration process between the electron injection and the backward transfer, whereas the other two dyes can establish the dynamic equilibrium between the linkage and divorce, which retards the backward transfer and, therefore, behave as a steady increase in H_2 evolution upon prolonging the irradiation time.

The present improved sensitizers, i.e., $Ru(bpy)_2(him)_2$-NO_3 and $Ru_2(bpy)_4L_1$-PF_6, have pronounced higher H_2 evolution efficiency and preferable durability. The best photosensitization of $Ru_2(bpy)_4L_1$-PF_6 is a demonstration of the operation of the "antenna effect" in the *m*-TiO_2 sensitization process. It

indicates that the conversion efficiency of absorbed light to H_2 is constant throughout the spectrum regardless of whether the incident light is absorbed by the linked unit or by the terminal ones. Namely, the light absorbed by the peripheral unit is efficiently transferred to the linked one, where it is used for the electron injection. The specific feature of the antenna-sensitizer is that, in addition to the visible light absorption by the sensitizer fragment, the high absorption of the antenna fragments can also be utilized for light harvesting and sensitization, which can be transferred through the MMCT [7]. Apparently, these results suggested interesting possibilities for the preparation of more efficient complex dyes with better durability, and effective dynamic equilibrium between the linkage of ground state dye and divorce of the oxidized dye is helpful to hinder the backward transfer and improve the quantum efficiency. This approach to the design of a dye-sensitized photocatalyst for H_2 production is both theoretically sound and practically effective. Research in this area is currently in progress.

4. Conclusions

This work shows that efficient H_2 production over the dye-sensitized Pt/*m*-TiO_2 nanoparticles suspension proceeded under visible light irradiation by using methanol as electron donors. The studied three types of Ru(II) bipyridyl complexes, which were attached to the Pt/*m*-TiO_2 through different linkage modes, show different photosensitization. N719 tightly bound to *m*-TiO_2 has better durability against photodeterioration but the lowest H_2 evolution efficiency, whereas the loosely attached $Ru(bpy)_2(him)_2$-NO_3 and $Ru_2(bpy)_4L_1$-PF_6 have pronounced higher H_2 evolution and preferable durability. The dynamic equilibrium between the linkage of the ground state dye and divorce of the oxidized dye seems to play a crucial role in the photochemical behavior in the dye-sensitized Pt/*m*-TiO_2 suspension, which can promote the electron injection and hinder the backward transfer, and then, improve the H_2 evolution efficiency.

The more steady and higher increase in H_2 evolution for $Ru_2(bpy)_4L_1$-PF_6 sensitized Pt/*m*-TiO_2 indicates that the "antenna effect" and the oxygen bridge linking with TiO_2 of this dye can enhance the visible light harvesting, electron injection efficiency, and then improve the photocatalytic H_2 evolution. These results suggested that it is possible to prepare more efficient complex dyes. These dyes can couple both the functions of a sensitizer which can be linked with the surface of TiO_2 to inject the photoelectron, and an antenna to realize the intramolecular energy transfer from highly absorbing chromophoric groups by tuning the molecular components. The use of above antenna-sensitizer may constitute a viable strategy to overcome problems of light harvesting efficiency for the H_2 evolution in the sensitization of wide-band gap semiconductors. Moreover, the effect of the linkage mode between the dye molecules and photocatalysts must be taken into account in constructing an effective dye-sensitized photocatalyst for H_2 production.

Acknowledgments

This work was supported by the National "863" Foundation of China (2006AA03Z344), Natural Science Foundation of China (20573078), Program for New Century Excellent Talents in University (NCET-07-0637) and Talented Young Scientist Foundation (2006ABB003) of Hubei Province, China.

References

[1] A. Fujishima, K. Honda, Nature (London) 238 (1972) 37–38.
[2] P.G. Hoertz, T.E. Mallouk, Inorg. Chem. 44 (2005) 6828–6840.
[3] M.K. Tian, W.F. Shangguan, J. Yuan, L. Jiang, M.X. Chen, J.W. Shi, Z.Y. Ouyang, S.J. Wang, Appl. Catal. A 309 (2006) 76–84.
[4] H.B. Song, T.Y. Peng, P. Cai, H.B. Yi, C.H. Yan, Catal. Lett. 113 (2007) 54–58.
[5] A. Kudo, Int. J. Hydrogen Energy 31 (2006) 197–202.
[6] Z.G. Zou, J.H. Ye, K. Sayama, H. Arakawa, Nature 414 (2001) 625–627.
[7] R. Amadelli, R. Argazzi, C.A. Bignozzi, F. Scandola, J. Am. Chem. Soc. 112 (1999) 7099–7103.
[8] H. Gerisher, J. Photochem. Photobiol. 16 (1972) 243–260.
[9] J. Kiwi, M. Graetzel, J. Am. Chem. Soc. 101 (1979) 7214–7217.
[10] H. Misawa, H. Sakuragi, Y. Usui, K. Tokumaru, Chem. Lett. (1983) 1021–1024.
[11] T. Kajiwara, K. Hashimoto, T. Kawai, T. Sakata, J. Phys. Chem. 86 (1982) 4516–4522.
[12] T. Shimizu, T. Iyoda, Y. Koide, J. Am. Chem. Soc. 107 (1985) 35–41.
[13] R. Abe, K. Hara, K. Sayama, K. Domen, H. Arakawa, J. Photochem. Photobiol. 37A (2000) 63–69.
[14] R. Abe, K. Sayama, H. Sugihara, J. Sol. Energy Eng. 127 (2005) 413–416.
[15] Y. Kim, S. Salim, M.J. Huq, T.E. Mallouk, J. Am. Chem. Soc. 113 (1991) 9561–9563.
[16] Y. Kim, S.J. Atherton, E.S. Brigham, T.E. Mallouk, J. Phys. Chem. 97 (1993) 11802–11810.
[17] R. R. Abe, K. Sayama, K. Domen, H. Arakawa, Chem. Phys. Lett. 379 (2003) 230–235.
[18] R. Abe, K. Sayama, H. Arakawa, Chem. Phys. Lett. 362 (2002) 441–444.
[19] K. Sayama, K. Mukasa, R. Abe, Y. Abe, H. Arakawa, Chem. Commun. (Cambridge) (2001) 2416–2417.
[20] T.Y. Peng, D. Zhao, K. Dai, W. Shi, K. Hirao, J. Phys. Chem. B 109 (2005) 4947–4952.
[21] T.Y. Peng, D. Zhao, H.B. Song, C.H. Yan, J. Mol. Catal. A: Chem. 238 (2005) 119–126.
[22] H.B. Yi, T.Y. Peng, D.N. Ke, D. Ke, L. Zan, C.H. Yan, Int. J. Hydrogen Energy 33 (2008) 672–678.
[23] S. Faham, M.W. Day, W.B. Connick, B.R. Crane, B. Di, J. Angel, W.P. Schaefer, D.C. Rees, H.B. Gray, Acta Crystallogr., D: Bio. Cryst. 55D (1999) 379–385.
[24] P. Cai, M.X. Li, C.Y. Duan, F. Lu, D. Guo, Q.J. Meng, New J. Chem. 29 (2005) 1011–1015.
[25] R. Abe, K. Sayama, K. Domen, H. Arakawa, Chem. Phys. Lett. (2001) 339–344.
[26] Z.G. Zou, H. Arakawa, J. Photochem. Photobiol. A 158 (2003)145–162.
[27] R. Abe, K. Sayama, H. Sugihara, J. Phys. Chem. B 109 (2005) 16052–16061.
[28] J.M. Herrmann, J. Disdier, P. Pichat, J. Phys. Chem. 90 (1998) 6028–6034.
[29] W.F. Shangguan, A. Yoshida, Int. J. Hydrogen Energy 24 (1999) 425–431.
[30] A. Hagfeldtt, M. Gratzel, Chem. Rev. 95 (1995) 49–68.
[31] B. O'Regan, M. Graetzel, Nature (London) 353 (1991) 737–740.
[32] K. Hara, Y. Tachibana, Y. Ohga, A. Shinpo, S. Suga, K. Sayama, H. Sugihara, H. Arakawa, Sol. Energy Mater. Sol. Cells 77 (2003) 89–103.
[33] T. Osa, M. Fujihira, Nature 264 (1976) 349–350.